Vertical Structure of Tropical Waves Maintained by Internally-Induced Cumulus Heating

CHIH-PEI CHANG

Department of Meteorology, Naval Postgraduate School, Monterey, Calif. 93940

(Manuscript received 25 November 1975, in revised form 22 January 1976)

ABSTRACT

Solutions to the wave-CISK (conditional instability of the second kind with cumulus heating being induced by low-level internal wave convergence) system are obtained to study the vertical structure of marginally unstable waves. A diabatic heating profile is specified that resembles those observed and those theoretically derived from simple parameterization schemes. Upper and lower bounds for the vertical wavelength of the unstable waves under normal heating conditions are established through analysis of the frequency (stability) equation. The lower bound excludes the possibility of excitation or maintenance of short vertical wavelengths (relative to the vertical scale of heating) by wave-CISK. The calculated growth rates indicate that this result is basically insensitive to the vertical heating profile. The vertical structure of the most unstable waves is also computed and the possible roles played by CISK in large-scale tropical waves are discussed in light of these results.

1. Introduction

The possibility that large-scale waves with short vertical wavelengths may be excited in the tropical atmosphere has been raised by Lindzen (1967), who showed that the equatorially trapped, internal gravity and internal Rossby waves usually have a small positive equivalent depth and therefore a short vertical wavelength. Holton (1969, 1972a) later pointed out that such short vertical wavelengths, if they exist in the troposphere, would cause great difficulties for numerical weather prediction in the equatorial region because of the stringent requirement for high vertical resolution. Whether short vertical-scale waves actually have a significant presence in the tropical troposphere or not is unclear due to inadequate observations. Studies based on conventional radiosonde data (e.g., Wallace, 1971; and others) tend to suggest that most of the variance of the waves in the tropical troposphere is associated with vertical scales comparable to the scale height. However, Madden and Zipser's (1970) analysis of high-resolution rawinsonde data obtained during the Line Island Experiment showed that a quite short vertical wavelength (~3 km) existed over the central equatorial Pacific. Further observational studies thus seem necessary to resolve this problem.

Condensation heating due to deep cumulus convection has been recognized as a primary energy source for large-scale tropical motions. Two possible mechanisms which may be responsible for the excitation of large-scale tropical waves by heating have been investigated. The first is a one-way forcing by the cumulus scale which receives no feedback from the large scale. Numerical study by Holton (1971, 1972a, 1973) and analytical work by Chang (1976) have shown that this mechanism excites tropical waves that have vertical scales comparable to those of the forcing, which are usually 10–14 km. The problem of short vertical wavelengths thus appears unimportant for forced waves. The second possible mechanism is the conditional instability of the second kind (CISK) which involves a feedback to cumulus convection by low-level convergence of large-scale motion. This low-level convergence may be due to frictionally induced cross-isobaric flow, as in the case of typhoons (which shall be called "Ekman-CISK"), or due to the structure of the internal waves (which shall be called "wave-CISK"). The Ekman-CISK has been shown by Chang (1971) and Chang and Piwowar (1974) to possess no preferred horizontal scale for synoptic wave disturbances. Thus Ekman-CISK may not explain the generation of synoptic-scale waves, but it may be quite important in maintaining the waves once they are initiated. The wave-CISK mechanism has been investigated by Hayashi (1970), Lindzen (1974) and Lindzen *et al.* (1975). Although Lindzen (1974) and Lindzen *et al.* (1975) found no direct horizontal scale selection, the most unstable wave-CISK mode has a vertical scale seemingly comparable to the depth of the sub-cloud layer or the low-level convergent moist layer, depending on the particular model aspects. A short vertical scale may therefore

Unauthenticated | Downloaded 05/21/24 04:42 PM UTC

be important for the excited waves. Using the calculated vertical scale they also speculated that, due to the Doppler-shifting effect of the variable basic flow and the small growth rates, a period of ~5 days associated with a wavenumber zero, mixed Rossby-gravity mode is likely to dominate the tropical spectra. This periodicity thus provides a basic frequency for tropical systems. Depending on the local basic flow, it may force resonantly higher wavenumbers that may be relevant to the observed waves.

Since the growth rates associated with wave-CISK are usually very small, it may be expected that the CISK waves have properties similar to neutrally forced waves. The difference in the selection of vertical scales between the forced models and the wave-CISK models thus appears to be worth further investigation. In addition to its importance for tropical numerical weather prediction, the vertical scale also determines other properties of the excited internal waves. The purpose of this paper is to examine the growth rates associated with wave-CISK, particularly with regard to the vertical scale selection mechanism.

2. Basic equations

Neglecting the shear of the mean zonal wind, the linearized zonal and meridional momentum, hydrostatic, thermodynamic energy and continuity equations for a single zonal wavenumber k on an equatorial beta-plane may be written

$$i\omega\hat{u}-\beta y\hat{v}=-ik\hat{\phi}, \tag{1}$$

$$i\omega\hat{v}+\beta y\hat{u}=-\frac{\partial\hat{\phi}}{\partial y}, \tag{2}$$

$$\frac{\partial\hat{\phi}}{\partial z}=\frac{R\hat{T}}{H}, \tag{3}$$

$$i\omega\hat{T}+\hat{w}\Gamma=\frac{\hat{Q}}{c_p}, \tag{4}$$

$$ik\hat{u}+\frac{\partial\hat{v}}{\partial y}+e^{z/H}\frac{\partial}{\partial z}(e^{-z/H}\hat{w})=0, \tag{5}$$

where $\hat{u}$, $\hat{v}$, $\hat{w}$, $\hat{T}$, $\hat{\phi}$ and $\hat{Q}$ are the perturbation zonal velocity, meridional velocity, vertical velocity, temperature, geopotential and diabatic heating rate, respectively; ω is the Doppler-shifted frequency, H a constant scale height, Γ the static stability, c_p the specific heat at constant pressure, R the gas constant, β the meridional gradient of the vertical component of earth's vorticity, y the meridional coordinate, and $z=-H\ln(p/p_0)$ is the vertical coordinate with p the pressure and p_0 a reference pressure.

Eqs. (1)–(5) may be combined into a single equation in $\hat{w}$ that may be separated into meridional and vertical structure equations by assuming that

$$\hat{w}=\sum_n Y_n(y)w_n(z)\exp[z/(2H)],$$

where the density factor $\exp[z/(2H)]$ is separated for convenience. The meridional structure equation is

$$\frac{d^2Y_n}{dy^2}+\left(\frac{k\beta}{\omega}-k^2+\frac{\omega^2}{gh_n}-\frac{\beta^2y^2}{gh_n}\right)Y_n=0, \tag{6}$$

where g is the gravitational constant and h_n, the equivalent depth, is the separation constant. Matsuno (1966) and Lindzen (1967) have shown that the solutions to (6) which satisfy the boundary condition

$$Y_n\to 0 \text{ as } |y|\to\infty, \tag{7}$$

and lead to the frequency equation

$$\left(\frac{k\beta}{\omega}-k^2+\frac{\omega^2}{gh_n}\right)\frac{(gh_n)^{\frac{1}{2}}}{\beta}=2n+1, \quad n=-1, 0, 1, 2, \ldots, \tag{8}$$

are

$$Y_n(y)=\left[\frac{n}{1-\frac{k}{\omega}(gh_n)^{\frac{1}{2}}}H_{n-1}(\xi)-\frac{1}{2\left[1+\frac{k}{\omega}(gh_n)^{\frac{1}{2}}\right]}H_{n+1}(\xi)\right]\times\exp(-\xi^2/2),$$

where $\xi\equiv\beta^{\frac{1}{2}}(gh_n)^{-\frac{1}{4}}y$ and the Hermite polynomials $H_n(\xi)$ have values only for $n\geq 0$. The meridional velocity solution is $v_n(y)\propto H_n(\xi)\exp(-\xi^2/2)$. Lamb (1973) has solved (6) using the more general form of the confluent hypergeometric functions without the restriction of (7). In such a case, the lateral boundary conditions are given by the choice of vanishing meridional velocity at some finite $|y|$ where the confluent hypergeometric functions have a node. The Hermite polynomials are a sub-set of the confluent hypergeometric functions.

The vertical structure equation which is most relevant in the present calculation is

$$\frac{d^2w_n}{dz^2}+\lambda_n^2w_n=\frac{Q_n'}{gh_n}, \tag{9}$$

where

$$\lambda_n^2=\frac{S}{gh_n}-\frac{1}{4H^2}, \tag{10}$$

$$S=\frac{R}{H}\Gamma,$$

$$Q_n'=\frac{R}{c_pH}\hat{Q}_nY_n^{-1}\exp[-z/(2H)].$$

Unauthenticated | Downloaded 05/21/24 04:42 PM UTC

The parameter λ_n is a measure of the vertical wavenumber and is generally complex for unstable waves. In the case of forced modes ω and k are known parameters of the forcing function so that h_n and λ_n are obtained from (8) and (10) respectively. For CISK modes, on the other hand, λ_n is determined as an eigenvalue of (9) and ω is then found from (8) and (10). In the present calculation, the heating function Q' is assumed to possess a white-noise distribution for all Hermite modes (all values of n) so that the calculation of h will be independent of n. The subscript n will therefore be dropped in the subsequent discussions. It is well known that the vertical structure equation (9) can also be derived by considering two-dimensional wave motion only.

As in the forced model by Chang (1976) the following boundary conditions are used to solve (9):

$$w=\begin{cases}0, & \text{at } z=0 \quad (11a)\\ C_1e^{i\lambda z}+C_2e^{-i\lambda z}, & \text{at } z=z_t \quad (11b)\end{cases}$$

where

$$C_1=rC_2.$$

Here z_t is the height of tropopause, C_1, C_2 are constants, and the condition (11b) results from the requirement that latent heating vanishes at z_t. The parameter r is a reflection coefficient which, in the absence of vertical wind shear, is given by the specification of the static stability distribution. If the heating is assumed to vanish below the cloud base (z_c), the solution to (9) may be written in the form

$$w(z)=-\frac{re^{i\lambda z}+e^{-i\lambda z}}{\lambda(1+r)}\int_{z_c}^{z_t}\sin\lambda z\frac{Q'}{gh}dz, \quad z\geqslant z_t, \quad (12a)$$

$$w(z)=-\frac{\sin\lambda z}{\lambda(1+r)}\int_{z}^{z_t}(re^{i\lambda z}+e^{-i\lambda z})\frac{Q'}{gh}dz-\frac{re^{i\lambda z}+e^{-i\lambda z}}{\lambda(1+r)}\times\int_{z_c}^{z}\sin\lambda z\frac{Q'}{gh}dz, \quad z_t>z>z_c, \quad (12b)$$

$$w(z)=-\frac{\sin\lambda z}{\lambda(1+r)}\int_{z_c}^{z_t}(re^{i\lambda z}+e^{-i\lambda z})\frac{Q'}{gh}dz, \quad z_c\geqslant z\geqslant 0. \quad (12c)$$

The solution procedure using the Green's function technique is the same as in Lindzen (1974).

3. The heating function

The parameterization of the effect of condensation heating due to cumulus convection is a major problem in tropical modeling. Important contributions on this problem have been made by the sophisticated schemes developed by Arakawa and Schubert (1974), Ooyama (1971), and others. On the other hand, in simplified analytical models, simpler schemes must be used to keep the mathematical analysis tractable. Usually in these models the vertical distribution of the heating is specified as a given function that is invariant in time. The major criticism of this type of parameterization is that the results are sensitive to the specified heating profile such that one can obtain the desired result by simply tuning the heating profile. Another criticism is that the inherent time-variation of the heating function due to the complicated scale interaction cannot be properly included. However, recent observational studies, using both the spectral analysis technique and the composite technique, have produced a consistent picture of the vertical heating profile due to latent heat release over the tropical oceanic areas. The profiles observed by Nitta (1970), Wallace (1971), Reed and Recker (1971) and Williams and Gray (1973) are plotted in Fig. 1. It can be seen that in each case a maximum occurs in the middle troposphere between the 6 and 9 km levels. On the other hand, observational analysis of the divergence and vertical velocity by Schubert and Reed (1975) using recent GATE data has yielded a result that implies a vertical heating profile different from those shown in Fig. 1. They found that the maximum vertical velocity, which usually coincides with the maximum heating, based on scaling arguments (Holton, 1972b), occurs at a much lower level. However, analyses of the same data set by Petrossiants *et al.* (1975) and Antsipovich *et al.* (1975) of the USSR Hydrometeorological Center have resulted in profiles which are in close agreement with Fig. 1. In any case, the profiles included in Fig. 1 are

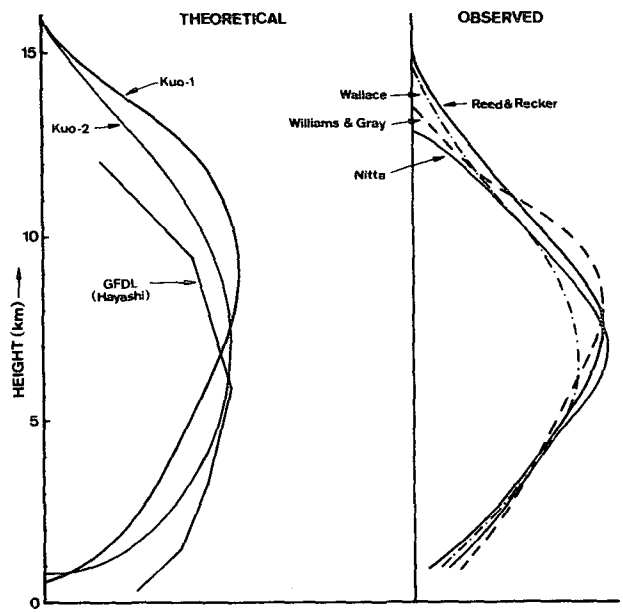

FIG. 1. Vertical heating functions deduced from observations and from simple theoretical parameterization schemes.

Unauthenticated | Downloaded 05/21/24 04:42 PM UTC

based on a much larger sample of data and may be viewed as an indication that the tropical atmosphere, on a *statistical basis*, tends to maintain a similar vertical profile for the large-scale heating function.

Results of a theoretical calculation by Kuo (1965) using his parameterization scheme are also included in Fig. 1. Kuo's parameterization was originally based on the assumption of horizontal mixing between cloud air and environmental air. Recently Kuo (1974) has shown that his formulation is equivalent to the consideration that heating is due to the adiabatic compression of the descending environment. Kuo's scheme has been used in many tropical numerical models with a degree of success not inferior to any other parameterization scheme. It is therefore interesting to compare his heating profiles with those observed. In Fig. 1, the Kuo-1 curve is for the case of no entrainment and the Kuo-2 curve is for the case of moderate entrainment. It is clear that the latter curve, having a maximum near 7 km, agrees quite well with those deduced from observations. The average heating profile obtained from the GFDL general circulation model as calculated by Hayashi (1973) is also included, because the GFDL model uses a different parameterization scheme: the moist convective adjustment. Hayashi decomposed the heating function into components of various equatorial beta-plane modes. Among them, the profile for the Kelvin waves ($n=-1$) at the equator is one of the curves least resembling those observed. This profile is also plotted in Fig. 1. It is seen that even for this highly simplified parameterization scheme the maximum heating still occurs near 6 km, within the range of the other curves.

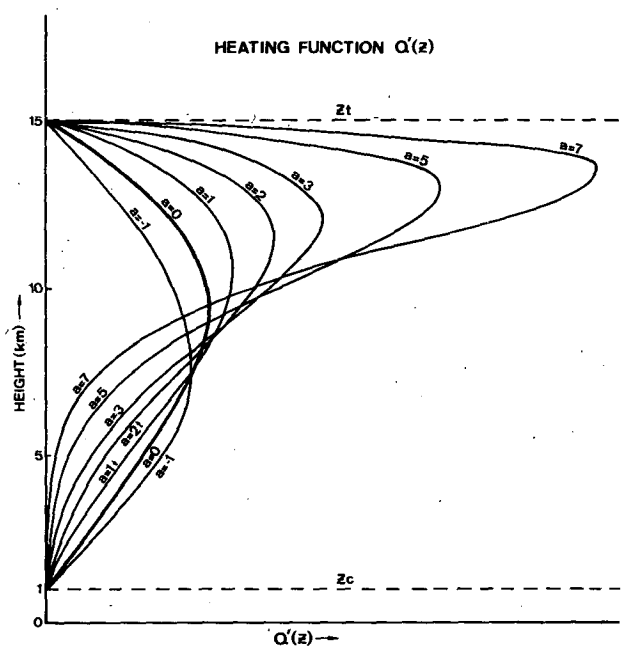

FIG. 2. The specified heating function $Q'(z)$.

Based on the above discussion the heating function for the wave-CISK parameterization is specified as

$$Q'(z)=\tfrac{1}{2}mNS_t w_b e^{az'}\sin\pi z', \quad z_t\geqslant z\geqslant z_c$$
$$Q'=0, \qquad z>z_t \text{ or } z<z_c \tag{13}$$

where

$$z'=\frac{z-z_c}{\Delta z},$$

and $\Delta z=z_t-z_c$ is a measure of the vertical scale of the heating. The coefficient m specifies the strength of the heating and the factor $\frac{1}{2}$ is needed because the amplitude of the Fourier component is one-half of the heating maximum, as only positive condensation heating is permitted. The heating is proportional to the moisture convergence in the moist layer which is represented by the vertical velocity w_b at the top of the moist layer. The tropospheric value of the static stability S_t is included in the proportionality constant. The parameter a is used to vary the maximum heating level to test the sensitivity of the model. The coefficient N is a normalization factor so that when other conditions are equal the total amount of heat release weighted by density in a column would remain the same with different values of a. Thus,

$$N=\frac{\int_0^1 \exp[-z/(2H)]dz'}{\int_0^1 \exp[az'-z/(2H)]\sin\pi z'dz'}$$
$$=\frac{2H\{1-\exp[-\Delta z/(2H)]\}\{[a-\Delta z/(2H)]^2+\pi^2\}}{\pi\{\exp[a-\Delta z/(2H)]+1\}}.$$

Profiles of (13) multiplied by the density factor $\exp(z/2H)$ are plotted in Fig. 2 for various values of a. The range of $-1\leqslant a\leqslant 0$, with maximum heating between 7 and 9 km, appears to be representative of the observed and theoretical profiles shown in Fig. 1.

4. Analysis of the stability equation

If the mixed layer with top at z_b ($<z_c$) is assumed to be the moisture layer which provides the convergence for CISK, the most relevant solution in studying the instability is (12c) evaluated at z_b. The solution is

$$w_b=-\frac{\sin\lambda z_b}{\lambda}\frac{\bar{m}w_b}{1+r}\frac{S_t}{gh}\frac{\pi\Delta z}{2}$$
$$\times\left[\frac{e^{-i\lambda z_c}(e^q+1)+re^{i\lambda z_c}(e^{-q}+1)}{q^2+\pi^2}\right],$$

where $\bar{m}=mN$ and $q=a-i\lambda\Delta z$. Equating the coefficients of w_b on both sides and using (10) leads to

Unauthenticated | Downloaded 05/21/24 04:42 PM UTC

the stability equation

$$\Psi(\lambda)\equiv\frac{\pi}{2}\bar{m}z_b\Delta z \times\frac{\left(\lambda^2+\frac{1}{4H^2}\right)[(e^q+1)e^{-i\lambda z_c}+r(e^{-q}+1)e^{-i\lambda z_c}]}{(1+r)(q^2+\pi^2)}+1=0, \tag{14}$$

where we have assumed that $(\sin\lambda z_b)/\lambda\approx z_b$. It can be shown that $q^2+\pi^2=0$ is not a solution to (14). Eq. (14) must be solved for the complex eigenvalue λ using either numerical or graphical methods. However, before doing so some valuable information regarding the range of vertical scale of the unstable solutions may be obtained by analyzing (14).

The complex eigenvalue λ may be written as $\lambda=\lambda_r+i\lambda_i$, where the real part λ_r is the vertical wavenumber while the imaginary part λ_i gives the growth rate of the waves. If the positive λ_r is chosen, the C_2 component in (11b) represents the downward phase or upward energy propagation and the C_1 component represents the upward phase or downward energy propagation. It then follows from (10) and (8) that if λ_i is negative, the imaginary part of the frequency ω will be negative and the waves will grow exponentially in time. Based on observations, and justified *a posteriori*, we shall consider only the case of marginally unstable waves, or very small growth rates. Thus the conditions applied to (14) may be written

$$\lambda_i=-|\lambda_i|, \tag{15}$$

$$\lambda_i^2\ll\lambda_r^2. \tag{16}$$

In addition, we shall assume

$$\lambda_r^2\gg\frac{1}{4H^2}, \tag{17}$$

which is valid for all practical purposes since the scale height H of the atmosphere is $\sim$7 km and (17) only places a restriction of $\sim$88 km for the maximum vertical wavelength.

Eq. (14) will now be analyzed by assuming that $a=0$ and that the stratosphere ($z>z_t$) and troposphere ($z\leqslant z_t$) have the same constant static stability S_t. In this case $r=0$ and since $q^2+\pi^2\neq0$ the stability equation may be re-written as

$$\Psi'(\lambda)=\Psi(\lambda)(q^2+\pi^2)=\frac{\pi}{2}\bar{m}z_b\Delta z\left(\lambda^2+\frac{1}{4H^2}\right)(e^q+1)\times\exp(-i\lambda_t z_c)+q^2+\pi^2=0.$$

Separating $\Psi'(\lambda)$ into its real and imaginary parts gives two equations:

$$\begin{aligned}\mathrm{Re}(\Psi')&=0,\\ \mathrm{Im}(\Psi')&=0.\end{aligned} \tag{18}$$

For $a=0$, (18) may be expanded to give

$$\mathrm{Re}(\Psi')=\left(\lambda_r^2-\lambda_i^2+\frac{1}{4H^2}\right)[\exp(\lambda_i z_t)\cos\lambda_r z_t+\exp(\lambda_i z_c)\cos\lambda_r z_c]+2\lambda_r\lambda_i[\exp(\lambda_i z_t)\sin\lambda_r z_t+\exp(\lambda_i z_c)\sin\lambda_r z_c]+\frac{2[\pi^2-\Delta z^2(\lambda_r^2-\lambda_i^2)]}{\pi\bar{m}z_b\Delta z}=0.$$

Simplifying this equation with the conditions (16) and (17) and using (15) lead to

$$\mathrm{Re}(\Psi')\approx\underbrace{(\lambda_r^2\cos\lambda_r z_t-2\lambda_r|\lambda_i|\sin\lambda_r z_t)\exp(-|\lambda_i|z_c)}_{\mathrm{I}}+\underbrace{(\lambda_r^2\cos\lambda_r z_c-2\lambda_r|\lambda_i|\sin\lambda_r z_c)\exp(-|\lambda_i|z_c)}_{\mathrm{II}}+\underbrace{\frac{2(\pi^2-\Delta z^2\lambda_r^2)}{\pi\bar{m}z_b\Delta z}}_{\mathrm{III}}=0. \tag{19}$$

Since $|\cos\lambda_r z_t|$, $|\sin\lambda_r z_t|$, $|\cos\lambda_r z_c|$ and $|\sin\lambda_r z_c|$ are all $\leqslant1$ and $\exp(-|\lambda_i|z_c)<1$, from (16) we have, allowing for small error under extreme cases,[1]

$$\left.\begin{aligned}|\mathrm{I}|&\leqslant\lambda_r^2\\ |\mathrm{II}|&\leqslant\lambda_r^2\end{aligned}\right\}. \tag{20}$$

Thus for (19) to be satisfied we may write

$$\mathrm{Max}[\mathrm{Re}(\Psi')]=\mathrm{Max}(\mathrm{I})+\mathrm{Max}(\mathrm{II})+\mathrm{III}>0,$$

where Max denotes the maximum value using the range (20):

$$\mathrm{Max}(\mathrm{I})=\mathrm{Max}(\mathrm{II})=\lambda_r^2.$$

Thus we have

$$2\lambda_r^2+\frac{2\pi}{\bar{m}z_b\Delta z}-\frac{2\Delta z\lambda_r^2}{\pi\bar{m}z_b}>0,$$

which yields

$$\lambda_r^2<\frac{\pi^2}{\Delta z(\Delta z-\pi\bar{m}z_b)}, \tag{21}$$

if

$$\Delta z>\pi\bar{m}z_b. \tag{22}$$

[1] The precise maximum for terms I and II is $\{|(1+4\epsilon^2)\cos[\tan^{-1}(-2\epsilon)|]\exp(-|\lambda_i|z_c)\}\lambda_r^2$, where $\epsilon=|\lambda_i/\lambda_r|$. Inequality (20) is true when $\epsilon=0$. For $\epsilon=0.1$ which is our assumption the maximum is $[1.02\exp(-|\lambda_i|z_c)]\lambda_r^2$. Obviously if $|\lambda_i|$ becomes large the exponential factor would become much less than 1.

Unauthenticated | Downloaded 05/21/24 04:42 PM UTC

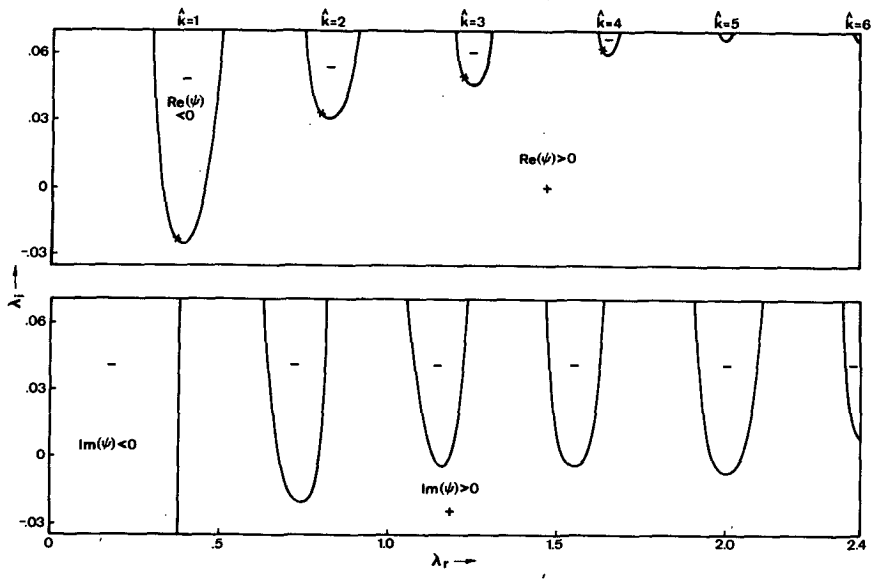

FIG. 3. Values of $\mathrm{Re}(\Psi)$ and $\mathrm{Im}(\Psi)$ as a function of $\lambda_r[\mathrm{km}^{-1}]$ and $\lambda_i[\mathrm{km}^{-1}]$. The crosses in the $\mathrm{Re}(\Psi)$ diagram are solutions for which $\mathrm{Re}(\Psi)=\mathrm{Im}(\Psi)=0$.

Choosing the minimum values (Min) in (20), we have

$$\mathrm{Min}[\mathrm{Re}(\Psi')]=\mathrm{Min}(\mathrm{I})+\mathrm{Min}(\mathrm{II})+\mathrm{III}<0,$$

or

$$-2\lambda_r^2+\frac{2\pi}{\bar{m}z_b\Delta z}-\frac{2\Delta z\lambda_r^2}{\pi\bar{m}z_b}<0,$$

giving

$$\lambda_r^2>\frac{\pi^2}{\Delta z(\Delta z+\pi\bar{m}z_b)}. \tag{23}$$

So (21) and (23) give the upper and lower bounds for λ_r. It is interesting to note that $\lambda_r\to\pi/\Delta z$ in the limit of $\bar{m}\to 0$, corresponding to a vertical wavelength of twice the heating scale, which is the most efficiently excited wavelength for forced waves (Chang, 1976). However, $\lambda_r=\pi/\Delta z$ cannot be a solution for any finite $\bar{m}$ because it does not satisfy (14).

Now we shall use the values $z_t=15$ km, $z_c=1$ km, $\Delta z=14$ km, $z_b=0.4$ km, $m=5.8$ which leads to $\bar{m}=9$. The value of m is calculated by fitting (13) to Reed and Recker's (1971) observed heating and vertical velocity profiles for the wave trough, for which an estimate of

$$mz_b\approx 2.32\ \mathrm{km}, \tag{24}$$

can be made assuming that $S_t=1.22\times10^{-4}\ \mathrm{s}^{-2}$ based on a tropospheric value of $\Gamma=3°\mathrm{C\ km}^{-1}$. Eq. (24) is a good approximation as long as $z_b<4$ km, so the particular choice of z_b is not crucial. From Reed and Recker's data $w_b\approx 0.29\ \mathrm{cm\ s}^{-1}$ so that the maximum heating is $\sim 6.8°\mathrm{C\ day}^{-1}$. Substituting these values into (21)–(23) we obtain

$$\frac{\pi}{6.14}=0.512>|\lambda_r|>\frac{\pi}{18.8}=0.167\ \mathrm{km}^{-1},$$

so the vertical wavelength, $L=2\pi/\lambda_r$, is limited by the following bounds:

$$13\ \mathrm{km}<L<40\ \mathrm{km}.$$

Thus waves with a vertical wavelength shorter than 13 km will not be excited by wave-CISK. If such waves are first excited by another mechanism, the above result indicates that they *cannot be maintained* by wave-CISK.

5. Eigenvalues and eigenfunctions

a. Growth rates

The stability equation (14) will now be solved using the graphical method with the accuracy of the solutions improved by a numerical iteration technique. The graphical method is illustrated in Fig. 3, where the real and imaginary parts of $\Psi(\lambda)$ given by (14) with $r=0$, $a=0$ and $m=6$ are plotted as a function of λ_r and λ_i. Here the constants used are $H=7$ km, $z_t=15$ km, $z_c=1$ km and $z_b=0.4$ km. The intersections of the zero $\mathrm{Re}(\Psi)$ and zero $\mathrm{Im}(\Psi)$ lines give the eigenvalue solution λ. It is seen that there exist many solutions with the most (and only) unstable solution having the smallest λ_r or the longest wavelength. The solutions are labeled by an integer $\hat{k}$ with increasing $\hat{k}$ indicating increased λ_r or decreased vertical wavelength.

The four longest vertical wavelength solutions are shown in Fig. 4 as a function of heating strength m. It is seen that $|\lambda_i|\ll\lambda_r$ and that the growth rates as represented by $-\lambda_i$ increase with m while the vertical wavelengths are almost constant. This diagram also indicates that the $\hat{k}=1$ solution is most unstable throughout the range $m=4$ to $m=10$, which cor-

Unauthenticated | Downloaded 05/21/24 04:42 PM UTC

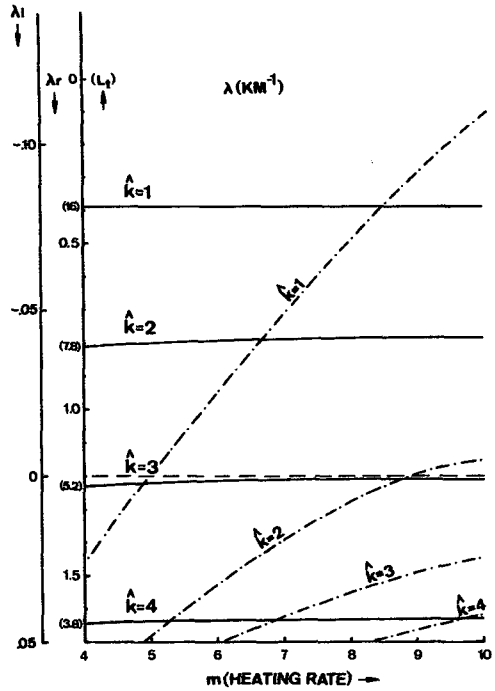

FIG. 4. The four longest vertical wavelength solutions as a function of the heating rate m. The solid curves are λ_r and the dash-dotted curves λ_i. The corresponding vertical wavelength $L_t=2\pi/\lambda_r$ is given in the parentheses of the λ_r coordinate. The ratio of static stabilities between stratosphere and troposphere is 1.

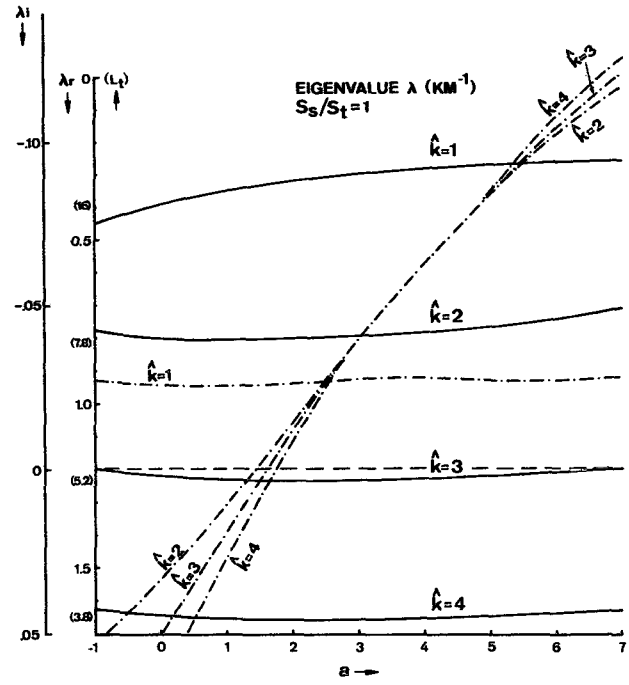

FIG. 5. As in Fig. 4 except that the solutions are given as a function of the heating profile parameter a.

responds to maximum heating rates of 4.7 and 11.7°C day^{-1} if $w_b=0.29$ cm s^{-1}. In fact, it is the only unstable solution up to $m=9$. For this solution the value of λ for $m=5.8$ is $0.388-0.026i$ [km^{-1}], which is well within the range predicted by (21) and (23).

The sensitivity of the eigenvalues with respect to the vertical heating profile (13) is shown in Fig. 5 in which the $\hat{k}=1$ to $\hat{k}=4$ solutions with $m=6$ are given as a function of a. It is clear that the vertical wavelengths are all insensitive to a. For the growth rates the $\hat{k}=1$ solution is almost independent of a, but the other solutions all increase with a. There is an indication that as a increased to >5 the shortest vertical wavelength becomes the most unstable solution. However, for the realistic range of $0\leqslant a\leqslant -1$, which represents the statistical mean state of the heating function in the tropical atmosphere, $\hat{k}=1$ is the only unstable solution.

Solutions for a different static stability S_s in the stratosphere are obtained by including the radiation condition for $z>z_t$ as the third boundary condition. In this case the reflection coefficient is derived by continuity requirements of w and ϕ across z_t:

$$r=\frac{1-(S_s/S_t)^{\frac{1}{2}}}{1+(S_s/S_t)^{\frac{1}{2}}}\exp(-2i\lambda_t z_t), \quad \text{for} \quad S_s>S_t.$$

The result for $S_s/S_t=2.5$ is shown in Fig. 6. It is seen that the general conclusions drawn from Fig. 5 remain valid, although waves with a shorter vertical wavelength become more unstable than the $\hat{k}=1$ waves beginning at $a=2$ which corresponds to a maximum

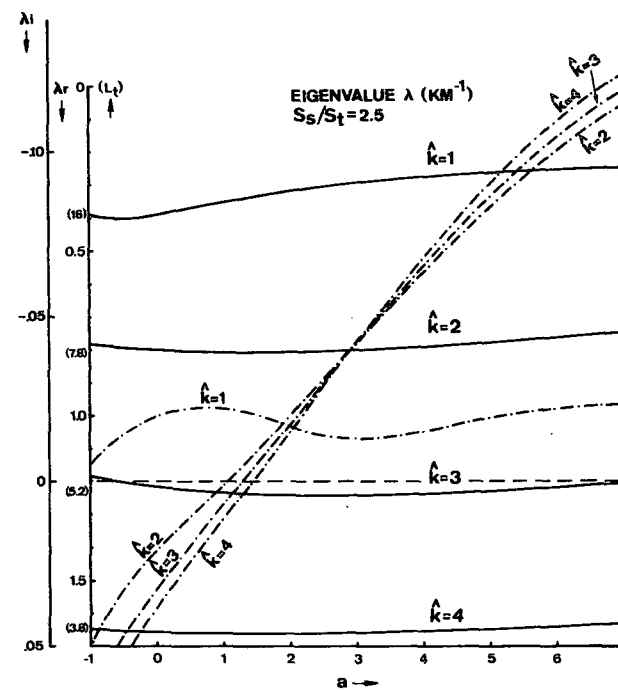

FIG. 6. As in Fig. 4 except that the solutions are given as a function of the heating profile parameter a and that the ratio of static stabilities between stratosphere and troposphere is 2.5.

Unauthenticated | Downloaded 05/21/24 04:42 PM UTC

heating level of ~12 km or 200 mb, much above all observed levels. So our result is basically insensitive to the vertical heating distribution.

b. Vertical profiles

The vertical structure of $\hat{w}$, corresponding to the λ for $\hat{k}=1$ and $a=0$ in Fig. 6, is shown in Fig. 7 for two heating intensities $m=6$ and 10. It can be seen that the tropospheric amplitude reaches a maximum between 6 and 9 km and has a minimum at the tropopause for both cases. In the stratosphere the amplitude for $m=6$ increases at a slow rate with height due to the density factor, but the kinetic energy actually decreases with height. This decrease is due to the instability of the waves which results in $\lambda_i<0$. The decrease of the wave kinetic energy is much faster for the more unstable $m=10$ case, so that even its amplitude decreases with height. The vertical phase distributions for both cases are almost the same and indicate that there is virtually no vertical propagation in the troposphere in contrast to a downward propagation in the stratosphere. The vertical wavelength computed from $2\pi/\lambda_r$ is 16.2 km in the troposphere and 10.2 km in the stratosphere, because the value of λ_r is increased in the stratosphere by approximately a factor of $(S_s/S_t)^{\frac{1}{2}}$, as can be seen from (10).

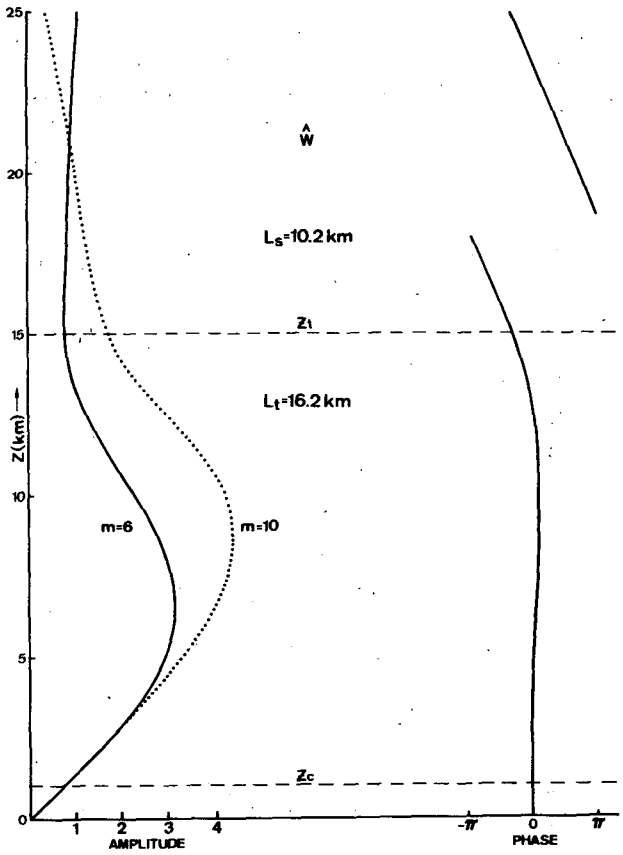

FIG. 7. Amplitude and phase of $\hat{w}$ as a function of height for $m=6$ (solid lines) and $m=10$ (dotted lines). The phase lines for both cases are approximately the same.

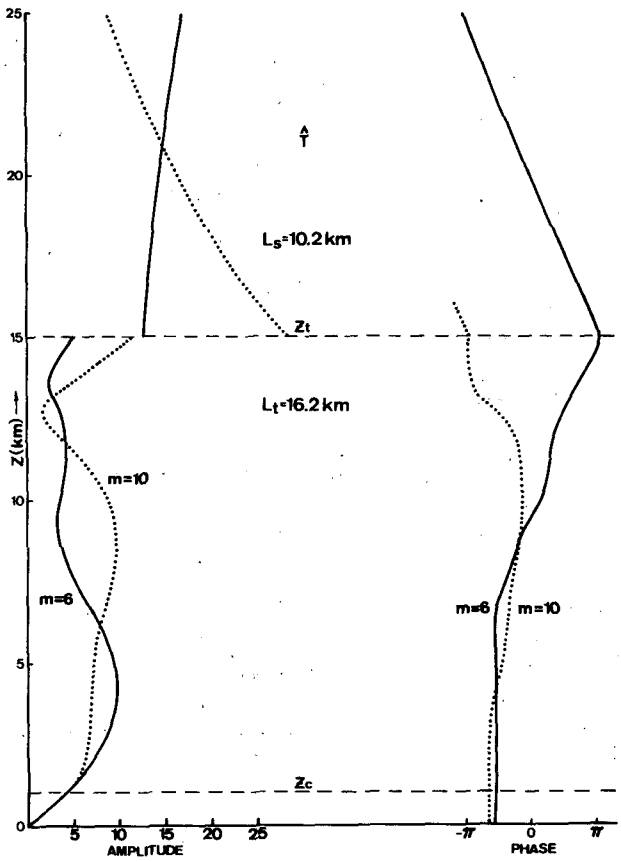

FIG. 8. As in Fig. 7 except for $\hat{T}$.

Vertical structures of other variables can be computed utilizing the basic equations (1)–(5) and the solutions to the meridional structure equation (6). Here only the temperature structure for the Kelvin wave case ($n=-1$) will be shown. From (4) and (8) we have

$$\hat{T}_{n=-1}=-\frac{i\left(\hat{w}S-\frac{R}{H}\frac{\hat{Q}}{c_p}\right)H}{kR(gh)^{\frac{1}{2}}}. \tag{25}$$

It is obvious from (25) that the amplitude of the temperature perturbation decreases as the zonal wavenumber k increases. The $\hat{T}_{n=-1}$ structure corresponding to the $\hat{w}$ in Fig. 7, is shown in Fig. 8. It can be seen that the amplitude distribution is quite sensitive to the strength of the heating. The discontinuity at z_t is due to the layered static stability distribution assumed in our model. The large temperature perturbations in the stratosphere are, of course, due to the large static stability there. Figs. 7 and 8 are constructed using nondimensional units. The two figures may be compared by letting the unit for the $\hat{w}$ amplitude be

Unauthenticated | Downloaded 05/21/24 04:42 PM UTC

1 cm s^{-1}; in this case the corresponding unit for the $\hat{T}$ amplitude will be α^{-1} [°C], where $\alpha=k\times$ (radius of the earth) is the number of waves around the equator. For these units the amplitude of $\hat{w}$ is quite close to the typically observed values of "matured" tropical waves, with maximum ~3 cm s^{-1} for $m=6$ and ~4.2 cm s^{-1} for $m=10$. On the other hand, the maximum $\hat{T}$ perturbation in the troposphere is almost 10°C for wavenumber (α) 1 and even larger in the stratosphere. Lindzen (personal communication) has suggested that these enormously large temperature fluctuations indicate that large damping effect of vertical momentum transport due to cumulus convection must be important. However, for shorter waves the temperature perturbation is proportionally smaller. If we consider a zonal wavelength of 4000 km, then $\alpha\approx 10$ and the temperature fluctuations are all <1°C in the troposphere, in good agreement with observations and with Holton (1971)'s numerical calculations. In fact, this magnitude estimate may explain why atmospheric Kelvin waves, which have a $\hat{T}$ amplitude ~2°C in the lower stratosphere, are not observed in the troposphere. For such waves the vertical velocity in the troposphere would be an order of magnitude smaller than for the easterly waves which have a typical zonal wavelength ~3000 km and a maximum vertical velocity ~3 cm s^{-1}. On the other hand, damping effect of a certain magnitude must play a role for the easterly waves to explain the complete absence of them in the stratosphere. Although these estimates are based on Kelvin waves only, for other wave modes a relationship between the tropospheric temperature amplitude and the zonal scale must also exist at latitudes somewhat away from the equator because of the following scaling arguments. Wallace (1971) and Holton (1972b) have shown that, for weak, tropical, synoptic-scale motions with a depth scale comparable to the scale height, a diabatic heating rate of 5–10°C day^{-1} is almost completely balanced by the adiabatic cooling. Thus the temperature fluctuation is one order of magnitude smaller than either term. This balance may be attributed to the smallness of the Rossby number which is ~O(1) or larger for tropical synoptic-scale motions. For planetary-scale motions the length scale is one order larger so that the Rossby number is ~$O(10^{-1})$ at intermediate tropical latitudes, and the scale analysis indicates that the pressure and temperature perturbations must be increased by one order of magnitude.

The phase diagrams in Figs. 7 and 8 indicate that in the lower troposphere and the entire stratosphere the temperature leads the vertical velocity by ~$\frac{1}{4}$ cycle. In the middle and upper troposphere (7–12 km for $m=6$ and 5–12 km for $m=10$), they are in phase except near the tropopause (12–14 km), where they are out of phase. These phase relationships are consistent with the energetics because the conditions for wave growth are

$$\int_0^\infty \overline{w'T'}dz>0,$$

$$\int_0^\infty \overline{Q'T'}dz>0.$$

From (25) and (10) it can be shown that these conditions are satisfied when $\lambda_i<0$ and

$$\int_0^\infty S\,\mathrm{Re}(\hat{w})dz<R\int_0^\infty \hat{Q}dz/(Hc_p).$$

The latter condition implies that the diabatic heating rate exceeds the adiabatic cooling rate which, of course, is responsible for the continuous growth of the waves with time.

c. Equatorial trapping scales

The meridional scale of the unstable waves may be estimated from the Hermite solutions of the meridional equation (6). The north-south, e-folding width is

$$y_e=\mathrm{Re}[2(gh)^{\frac{1}{2}}/\beta]^{\frac{1}{2}},$$

and the maximum amplitude for the mixed Rossby-gravity mode ($n=0$) occurs at

$$y_0=\mathrm{Re}[(gh)^{\frac{1}{2}}/\beta]^{\frac{1}{2}}.$$

The maximum for the Kelvin mode occurs at the equator. From results obtained for the $\hat{k}=1$ waves, $\lambda\approx 0.388-0.026i$ [km^{-1}] so that $(gh)^{\frac{1}{2}}\approx 25.5-1.7i$ [m s^{-1}] from (10). It follows that $y_e\approx 1480$ km and $y_0\approx 1050$ km with $\beta=2.21\times 10^{-11}$ m^{-1} s^{-1}. Both of these are reasonable values in terms of the trapping of waves on the equatorial beta-plane.

6. Concluding remarks

We have shown that tropical waves cannot remain unstable with respect to wave-CISK if the vertical wavelength is much smaller than the vertical scale of heating. This result holds for a number of reasonable heating profiles that have been observed or theoretically derived. The dispersive relationship of the growth rates of various equatorial beta-plane modes has been shown by Lindzen (1974) to be unsatisfactory in selecting the horizontal scale of tropical waves. From the computed eigenvalues it can be shown that, even under the extremely intense heating case of $m=10$, the growth rates for Rossby waves, mixed Rossby-gravity waves, and the longer zonal-scale Kelvin waves are all very small. This result is similar to that obtained by Chang and Piwowar (1974) for the Ekman-CISK and indicates that wave-CISK is not responsible for the initial selection mechanism of the tropical waves. Once the waves are excited

Unauthenticated | Downloaded 05/21/24 04:42 PM UTC

by some other mechanism, however, the internal wave convergence could induce organized cumulus convection and release wave-CISK as an energy source. The present calculation indicates that under such cases the shorter vertical-scale waves will still not be maintained by wave-CISK. There is no definite explanation to the fact that the gravity modes and the shorter zonal scale Kelvin modes, which are usually not observed in the tropical atmosphere, are most unstable. However, these waves have very short periods and various arguments have been given against their occurrence on a regular basis. For example, if one considers the lifting process[2] of CISK (Ooyama, 1969; Holton, 1972b), the short periods will be insufficient for a low-level air parcel to reach its condensation level. In any case, the result that wave-CISK can neither excite nor maintain waves with short vertical wavelengths remains valid independent of these considerations. The concern about short vertical-scale excitation due to wave-CISK in a tropical numerical model may thus be relieved. The resonant forcing of tropical waves by a fundamental wave-CISK frequency associated with the zonally-symmetric, mixed Rossby-gravity mode as hypothesized by Lindzen (1974) also does not appear to be plausible, because the equivalent depth would be too large to give a fundamental periodicity near 5 days.

The calculated vertical structure of $\hat{w}$ and $\hat{T}$ applies to all waves maintained by heating and is not restricted to wave-CISK. The eigenvalue λ found by the wave-CISK equation used here may alternatively be viewed as being excited by a specified forcing [as in the model by Chang (1976)] with a small linear damping. The damping coefficient would then appear in the complex Doppler-shifted frequency in the same way an an imaginary frequency due to instability. The computed magnitudes of $\hat{w}$ and $\hat{T}$ suggest that the observed planetary-scale Kelvin waves are likely to be a result of forcing rather than instability, because a small forcing function can explain the amplitudes in the stratosphere and troposphere. However, an instability consistent with the present CISK parameterization should eventually amplify the waves to a finite amplitude $\hat{w}$ comparable to that observed for large-scale, cumulus-associated tropical motions, but with a temperature amplitude too large to be realistic. The small low-level vertical velocities of these waves is also an indication that CISK is unlikely to be important. On the other hand, the tropospheric amplitude of the synoptic-scale waves may quite possibly be supported by a CISK-type process. These waves have a wavelength $\sim$2000–4000 km and a period $\sim$5 days which lead to a phase speed relative to the ground of $\sim$5–9 m s^{-1}. Such a phase speed would make the waves greatly attenuated before reaching the stratosphere, because the Doppler-shifted phase speed is very small near and below the tropopause and the damping can become very efficient (Lindzen, 1971).

[2] Lindzen *et al.* (1975) have alternatively considered that the CISK is not a lifting process but a low-level organizing process which does not require lifting.

Acknowledgments. The author wishes to thank Profs. R. T. Williams and R. L. Elsberry for reading the manuscript and making helpful suggestions. This research was supported by the Atmospheric Science Section, National Science Foundation, under Grant DES75-10719. Parts of the material in this paper were presented at the AMS Ninth Technical Conference on Hurricanes and Tropical Meteorology, May 1975, Miami, Fla.

REFERENCES

Antsipovich, V. A., A. I. Snitkovsky and A. I. Falkovich, 1975: On the orders of the values of the meterological elements obtained in the A/B-array in the period of GATE. GATE Rept., No. 14, Preliminary Scientific Results, Vol. 2, 99–116. [Available from WMO, Geneva].

Arakawa, A., and W. H. Schubert, 1974: Interaction of a cumulus cloud ensemble with the large-scale environment, Part I. *J. Atmos. Sci.*, **31**, 674–701.

Chang, C.-P., 1971: On the stability of low-latitude quasi-geostrophic flow in a conditionally unstable atmosphere. *J Atmos. Sci.*, **28**, 270–274.

——, 1976: Forcing of stratospheric Kelvin waves by tropospheric heat sources. *J. Atmos. Sci.*, **33**, 740–744.

——, and T. M. Piwowar, 1974: Effect of a CISK parameterizatino on tropical wave growth. *J. Atmos. Sci.*, **31**, 1256–1261.

Hayashi, Y., 1970: A theory of large-scale equatorial waves generated by condensation heat and accelerating the zonal wind. *J. Meteor. Soc. Japan*, **48**, 140–160.

——, 1973: Spectral analysis of tropical disturbances appearing in a GFDL general circulation model. *J. Atmos. Sci.*, **31**, 180–218.

Holton, J. R., 1969: A note on the scale analysis of tropical motions. *J. Atmos. Sci.*, **26**, 770–771.

——, 1971: A diagnostic model for equatorial wave disturbances: The role of vertical shear of the mean zonal wind. *J. Atmos. Sci.*, **28**, 55–64.

——, 1972a: Waves in the equatorial stratosphere generated by tropospheric heat sources. *J. Atmos. Sci.*, **29**, 368–375.

——, 1972b: *An Introduction to Dynamic Meteorology*. Academic Press, 319 pp.

——, 1973: On the frequency distribution of atmospheric Kelvin waves. *J. Atmos. Sci.*, **30**, 499–501.

Kuo, H.-L., 1965: On formation and intensification of tropical cyclones through latent heat release by cumulus convection. *J. Atmos. Sci.*, **22**, 40–63.

——, 1974: Further studies of parameterization of the influence of cumulus convection on large-scale flow. *J. Atmos. Sci.*, **31**, 1232–1240.

Lamb, V. R., 1973: The response of a tropical atmosphere to middle latitude forcing. Ph.D. thesis, University of California, Los Angeles, 151 pp.

Lindzen, R. S., 1967: Planetary waves on beta planes. *Mon. Wea. Rev.*, **95**, 441–445.

——, 1971: Equatorial planetary waves in shear: Part I. *J. Atmos. Sci.*, **28**, 609–622.

——, 1974: Wave-CISK in the tropics. *J. Atmos. Sci.*, **31**, 156–179.

——, L. Shapiro, D. Stevens and E. Sarachik, 1975: Tropical waves and oscillations. Paper presented at the Ninth Technical Conference on Hurricanes and Tropical Meteorology, Miami. (Abstract: *Bull. Amer. Meteor. Soc.*, **56**, 313–314).

Unauthenticated | Downloaded 05/21/24 04:42 PM UTC

Madden, R., and E. Zipser, 1970: Multi-layered structure of the wind over the equatorial Pacific during the Line Island Experiment. *J. Atmos. Sci.*, **27**, 336–342.

Matsuno, T., 1966: Quasi-geostrophic motions in the equatorial area. *J. Meteor. Soc. Japan*, **44**, 25–43.

Nitta, T., 1970: A study of generation and conversion of eddy available potential energy in the tropics. *J. Meteor. Soc. Japan*, **48**, 524–528.

Ooyama, K., 1969: Numerical simulation of the life cycle of tropical cyclones. *J. Atmos. Sci.*, **26**, 3–40.

——, 1971: A theory on parameterization of cumulus convection. *J. Meteor. Soc. Japan*, **49**, 744–756.

Petrossiants, M. A., A. I. Snitkovsky and A. I. Falkovich, 1975: On the evolution of the ITCZ. GATE Rept. No. 14, Preliminary Scientific Results, Vol. 1, 12–28. [Available from WMD, Geneva].

Reed, R. J., and E. E. Recker, 1971: Structure and properties of synoptic-scale wave disturbances in the equatorial western Pacific. *J. Atmos. Sci.*, **28**, 1117–1133.

Schubert, W. H., and R. J. Reed, 1975: Vertical motion and vorticity in the A/B scale area: Phase II. GATE Rept. No. 14, Preliminary Scientific Results, Vol. 1, 137–144. [Available from WMO, Geneva].

Wallace, J. M., 1971: Spectral studies of tropospheric wave disturbances in the tropical western Pacific. *Rev. Geophys. Space Phys.*, **9**, 557–612.

Williams, K. T., and W. M. Gray, 1973: Statistical analysis of satellite observed trade wind cloud clusters in the western North Pacific. *Tellus*, **25**, 313–336.

Unauthenticated | Downloaded 05/21/24 04:42 PM UTC